

1 **MitoChime: A Machine-Learning Pipeline for**
2 **Detecting PCR-Induced Chimeras in**
3 **Mitochondrial Illumina Reads**

4 A Special Project Proposal
5 Presented to
6 the Faculty of the Division of Physical Sciences and Mathematics
7 College of Arts and Sciences
8 University of the Philippines Visayas
9 Miag-ao, Iloilo

10 In Partial Fulfillment
11 of the Requirements for the Degree of
12 Bachelor of Science in Computer Science

13 by

14 Duranne Duran
15 Yvonne Lin
16 Daniella Pailden

17 Adviser
18 Francis D. Dimzon, Ph.D.

19 December 5, 2025

Contents

21	1 Introduction	1
22	1.1 Overview	1
23	1.2 Problem Statement	3
24	1.3 Research Objectives	4
25	1.3.1 General Objective	4
26	1.3.2 Specific Objectives	4
27	1.4 Scope and Limitations of the Research	5
28	1.5 Significance of the Research	6
29	2 Review of Related Literature	7
30	2.1 The Mitochondrial Genome	7
31	2.1.1 Mitochondrial Genome Assembly	8

32	2.2 PCR Amplification and Chimera Formation	9
33	2.3 Existing Traditional Approaches for Chimera Detection	10
34	2.3.1 UCHIME	11
35	2.3.2 UCHIME2	13
36	2.3.3 CATch	14
37	2.3.4 ChimPipe	15
38	2.4 Machine Learning Approaches for Chimera and Sequence Quality	
39	Detection	16
40	2.4.1 Feature-Based Representations of Genomic Sequences . . .	17
41	2.5 Synthesis of Chimera Detection Approaches	18
42	3 Research Methodology	22
43	3.1 Research Activities	22
44	3.1.1 Data Collection	23
45	3.1.2 Bioinformatics Tools Pipeline	27
46	3.1.3 Machine Learning Model Development	30
47	3.1.4 Model Benchmarking, Hyperparameter Optimization, and	
48	Evaluation	31
49	3.1.5 Feature Importance and Interpretation	32

50	3.1.6 Validation and Testing	33
51	3.1.7 Documentation	34
52	3.2 Calendar of Activities	35

⁵³ List of Figures

⁵⁴	3.1 Process Diagram of Special Project	23
---------------	--	----

⁵⁵ List of Tables

⁵⁶	2.1 Summary of Existing Methods and Research Gaps	20
⁵⁷	3.1 Timetable of Activities	35

⁵⁸ **Chapter 1**

⁵⁹ **Introduction**

⁶⁰ **1.1 Overview**

⁶¹ The rapid advancement of next-generation sequencing (NGS) technologies has
⁶² transformed genomic research by enabling high-throughput and cost-effective
⁶³ DNA analysis (Metzker, 2010). Among current platforms, Illumina sequencing
⁶⁴ remains the most widely adopted, capable of producing millions of short reads
⁶⁵ that can be assembled into reference genomes or analyzed for genetic variation
⁶⁶ (Bentley et al., 2008; Glenn, 2011). Despite its high base-calling accuracy,
⁶⁷ Illumina sequencing is prone to artifacts introduced during library preparation,
⁶⁸ particularly polymerase chain reaction (PCR)-induced chimeras, which are ar-
⁶⁹ tificial hybrid sequences that do not exist in the true genome (Judo, Wedel, &
⁷⁰ Wilson, 1998).

⁷¹ PCR chimeras form when incomplete extension products from one template

72 anneal to an unrelated DNA fragment and are extended, creating recombinant
73 reads (Qiu et al., 2001). In mitochondrial genome assembly, such artifacts are
74 especially problematic because the mitochondrial genome is small, circular, and
75 often repetitive (Boore, 1999; Cameron, 2014). Even a small number of chimeric
76 or misjoined reads can reduce assembly contiguity and introduce false junctions
77 during organelle genome reconstruction (Dierckxsens, Mardulyn, & Smits, 2017;
78 Hahn, Bachmann, & Chevreux, 2013; Jin et al., 2020). Existing assembly tools
79 such as GetOrganelle and MITObim assume that input reads are largely free of
80 such artifacts (Hahn et al., 2013; Jin et al., 2020). Consequently, undetected
81 chimeras may produce fragmented assemblies or misidentified organellar bound-
82 aries. To ensure accurate reconstruction of mitochondrial genomes, a reliable
83 method for detecting and filtering PCR-induced chimeras before assembly is es-
84 sential.

85 This study focuses on mitochondrial sequencing data from the genus *Sar-*
86 *dinella*, a group of small pelagic fishes widely distributed in Philippine waters.
87 Among them, *Sardinella lemuru* (Bali sardinella) is one of the country's most
88 abundant and economically important species, providing protein and livelihood
89 to coastal communities (Labrador, Agmata, Palermo, Ravago-Gotanco, & Pante,
90 2021; Willette, Bognot, Mutia, & Santos, 2011). Accurate mitochondrial assem-
91 blies are critical for understanding its population genetics, stock structure, and
92 evolutionary history. However, assembly pipelines often encounter errors or fail
93 to complete due to undetected chimeric reads. To address this gap, this research
94 introduces MitoChime, a machine learning pipeline designed to detect and filter
95 PCR-induced chimeric reads using both alignment-based and sequence-derived
96 statistical features. The tool aims to provide bioinformatics laboratories, partic-

97 ularly the Philippine Genome Center Visayas (PGC Visayas), with an efficient
98 solution for improving mitochondrial genome reconstruction.

99 1.2 Problem Statement

100 While NGS technologies have revolutionized genomic data acquisition, the ac-
101 curacy of mitochondrial genome assembly remains limited by artifacts produced
102 during PCR amplification. These chimeric reads can distort assembly graphs and
103 cause misassemblies, with particularly severe effects in small, circular mitochon-
104 drial genomes (Boore, 1999; Cameron, 2014). Existing assembly pipelines such
105 as GetOrganelle, MITObim, and NOVOPlasty assume that sequencing reads are
106 free of such artifacts (Dierckxsens et al., 2017; Hahn et al., 2013; Jin et al., 2020).
107 At PGC Visayas, several mitochondrial assemblies have failed or yielded incom-
108 plete contigs despite sufficient coverage, suggesting that undetected chimeric reads
109 compromise assembly reliability. Meanwhile, existing chimera detection tools such
110 as UCHIME and VSEARCH were developed primarily for amplicon-based com-
111 munity analysis and rely heavily on reference or taxonomic comparisons (Edgar,
112 Haas, Clemente, Quince, & Knight, 2011; Rognes, Flouri, Nichols, Quince, &
113 Mahé, 2016). These approaches are unsuitable for single-species organellar data,
114 where complete reference genomes are often unavailable. Therefore, there is a
115 pressing need for a reference-independent, data-driven tool capable of detecting
116 and filtering PCR-induced chimeras in mitochondrial sequencing datasets.

₁₁₇ **1.3 Research Objectives**

₁₁₈ **1.3.1 General Objective**

₁₁₉ This study aims to develop and evaluate a machine learning-based pipeline (Mi-
₁₂₀ toChime) that detects PCR-induced chimeric reads in *Sardinella lemuru* mito-
₁₂₁ chondrial sequencing data in order to improve the quality and reliability of down-
₁₂₂ stream mitochondrial genome assemblies.

₁₂₃ **1.3.2 Specific Objectives**

₁₂₄ Specifically, the study aims to:

- ₁₂₅ 1. construct simulated *Sardinella lemuru* Illumina paired-end datasets contain-
₁₂₆ ing both clean and PCR-induced chimeric reads,
- ₁₂₇ 2. extract alignment-based and sequence-based features such as k-mer compo-
₁₂₈ sition, junction complexity, and split-alignment counts from both clean and
₁₂₉ chimeric reads,
- ₁₃₀ 3. train, validate, and compare supervised machine-learning models for classi-
₁₃₁ fying reads as clean or chimeric,
- ₁₃₂ 4. determine feature importance and identify indicators of PCR-induced
₁₃₃ chimerism,
- ₁₃₄ 5. integrate the optimized classifier into a modular and interpretable pipeline
₁₃₅ deployable on standard computing environments at PGC Visayas.

136 1.4 Scope and Limitations of the Research

137 This study focuses on detecting PCR-induced chimeric reads in Illumina paired-
138 end mitochondrial sequencing data from *Sardinella lemuru*. The decision to re-
139 strict the taxonomic scope to a single species is based on four considerations:
140 (1) to limit interspecific variation in mitochondrial genome size, GC content, and
141 repetitive regions so that differences in read patterns can be attributed more di-
142 rectly to PCR-induced chimerism; (2) to align the analysis with relevant *S. lemuru*
143 sequencing projects at PGC Visayas; (3) to take advantage of the availability of *S.*
144 *lemuru* mitochondrial assemblies and raw datasets in public repositories such as
145 the National Center for Biotechnology Information (NCBI), which facilitates refer-
146 ence selection and benchmarking; and (4) to develop a tool that directly supports
147 local studies on *S. lemuru* population structure and fisheries management.

148 The study emphasizes `wgsim`-based simulations and selected empirical mito-
149 chondrial datasets from *S. lemuru*. It excludes naturally occurring chimeras, nu-
150 clear mitochondrial pseudogenes (NUMTs), and large-scale assembly rearrange-
151 ments in nuclear genomes. Feature extraction is restricted to low-dimensional
152 alignment and sequence statistics, such as k-mer frequency profiles, GC content,
153 read length, soft and hard clipping metrics, split-alignment counts, and map-
154 ping quality, rather than high-dimensional deep learning embeddings. This de-
155 sign keeps model behaviour interpretable and ensures that the pipeline can be
156 run on standard workstations at PGC Visayas. Testing on long-read platforms
157 (e.g., Nanopore, PacBio) and other taxa is outside the scope of this project; the
158 implemented pipeline is evaluated only on short-read *S. lemuru* datasets.

¹⁵⁹ 1.5 Significance of the Research

¹⁶⁰ This research provides both methodological and practical contributions to mi-
¹⁶¹tochondrial genomics and bioinformatics. First, MitoChime filters PCR-induced
¹⁶² chimeric reads prior to genome assembly, with the goal of improving the con-
¹⁶³tiguity and correctness of *Sardinella lemuru* mitochondrial assemblies. Second,
¹⁶⁴ it replaces informal manual curation with a documented workflow, improving au-
¹⁶⁵tomation and reproducibility. Third, the pipeline is designed to run on computing
¹⁶⁶ infrastructures commonly available in regional laboratories, enabling routine use
¹⁶⁷ at facilities such as PGC Visayas. Finally, more reliable mitochondrial assemblies
¹⁶⁸ for *S. lemuru* provide a stronger basis for downstream applications in the field of
¹⁶⁹ fisheries and genomics.

¹⁷⁰ **Chapter 2**

¹⁷¹ **Review of Related Literature**

¹⁷² This chapter presents an overview of the literature relevant to the study. It
¹⁷³ discusses the biological and computational foundations underlying mitochondrial
¹⁷⁴ genome analysis and assembly, as well as existing tools, algorithms, and techniques
¹⁷⁵ related to chimera detection and genome quality assessment. The chapter aims to
¹⁷⁶ highlight the strengths, limitations, and research gaps in current approaches that
¹⁷⁷ motivate the development of the present study.

¹⁷⁸ **2.1 The Mitochondrial Genome**

¹⁷⁹ Mitochondrial genome (mtDNA) is a small, typically circular molecule found in
¹⁸⁰ most eukaryotes. It encodes essential genes involved in oxidative phosphorylation
¹⁸¹ and energy metabolism. Because of its conserved structure, mtDNA has become
¹⁸² a valuable genetic marker for studies in population genetics and phylogenetics
¹⁸³ (Anderson et al., 1981; Boore, 1999). In animal species, the mitochondrial genome

ranges from 15–20 kilobase and contains 13 protein-coding genes, 22 tRNAs, and two rRNAs arranged compactly without introns (Gray, 2012). In comparison to nuclear DNA, the ratio of the number of copies of mtDNA is higher and has simple organization which make it particularly suitable for genome sequencing and assembly studies (Dierckxsens et al., 2017).

2.1.1 Mitochondrial Genome Assembly

Mitochondrial genome assembly refers to the reconstruction of the complete mitochondrial DNA (mtDNA) sequence from raw or fragmented sequencing reads. It is conducted to obtain high-quality, continuous representations of the mitochondrial genome that can be used for a wide range of analyses, including species identification, phylogenetic reconstruction, evolutionary studies, and investigations of mitochondrial diseases. Because mtDNA evolves rapidly, its assembled sequence provides valuable insights into population structure, lineage divergence, and adaptive evolution across taxa (Boore, 1999). Compared to nuclear genome assembly, assembling the mitochondrial genome is often considered more straightforward but still encounters technical challenges such as the formation of chimeric reads. Commonly used tools for mitogenome assembly such as GetOrganelle and MITObim operate under the assumption of organelle genome circularity, and are vulnerable when chimeric reads disrupt this circular structure, resulting in assembly errors (Hahn et al., 2013; Jin et al., 2020).

204 2.2 PCR Amplification and Chimera Formation

205 PCR plays an important role in NGS library preparation, as it amplifies target
206 DNA fragments for downstream analysis. However as previously mentioned, the
207 amplification process can also introduce chimeric reads which compromises the
208 quality of the input reads supplied to sequencing or assembly workflows. Chimeras
209 typically arise when incomplete extension occurs during a PCR cycle. This causes
210 the DNA polymerase to switch from one template to another and generate hy-
211 brid recombinant molecules (Judo et al., 1998). Artificial chimeras are produced
212 through such amplification errors, whereas biological chimeras occur naturally
213 through genomic rearrangements or transcriptional events.

214 In the context of amplicon-based sequencing, the presence of chimeras can in-
215 flate estimates of genetic or microbial diversity and may cause misassemblies dur-
216 ing genome reconstruction. Qin et al. (2023) has reported that chimeric sequences
217 may account for more than 10% of raw reads in amplicon datasets. This artifact
218 tends to be most prominent among rare operational taxonomic units (OTUs) or
219 singletons, which are sometimes misinterpreted as novel diversity, further caus-
220 ing the complication of microbial diversity analyses (Gonzalez, Zimmermann, &
221 Saiz-Jimenez, 2004). As such, determining and minimizing PCR-induced chimera
222 formation is vital for improving the quality of mitochondrial genome assemblies,
223 and ensuring the reliability of amplicon sequencing data.

224 **2.3 Existing Traditional Approaches for Chimera**

225 **Detection**

226 Several computational tools have been developed to identify chimeric sequences in
227 NGS datasets. These tools generally fall into two categories: reference-based and
228 de novo approaches. Reference-based chimera detection, also known as database-
229 dependent detection, is one of the earliest and most widely used computational
230 strategies for identifying chimeric sequences in amplicon-based community studies.
231 These methods rely on the comparison of each query sequence against a curated,
232 high-quality database of known, non-chimeric reference sequences (Edgar et al.,
233 2011).

234 On the other hand, the de novo chimera detection, also referred to as reference-
235 free detection, represents an alternative computational paradigm that identifies
236 chimeric sequences without reliance on external reference databases. This method
237 infer chimeras based on internal relationships among the sequences present within
238 the dataset itself, making it particularly advantageous in studies of under explored
239 or taxonomically diverse communities where comprehensive reference databases
240 are unavailable or incomplete (Edgar, 2016; Edgar et al., 2011). The underlying
241 assumption on this method is that during PCR, true biological sequences are
242 generally more abundant as they are amplified early and dominate the read pool,
243 whereas chimeric sequences appear later and are generally less abundant. The
244 de novo approach leverage this abundance hierarchy, treating the most abundant
245 sequences as supposed parents and testing whether less abundant sequences can
246 be reconstructed as mosaics of these templates. Compositional and structural
247 similarity are also evaluated to check whether different regions of a candidate

248 sequence correspond to distinct high-abundance sequences.

249 In practice, many modern bioinformatics pipelines combine both paradigms
250 sequentially: an initial de novo step identifies dataset-specific chimeras, followed
251 by a reference-based pass that removes remaining artifacts relative to established
252 databases (Edgar, 2016). These two methods of detection form the foundation of
253 tools such as UCHIME and later UCHIME2.

254 2.3.1 UCHIME

255 Developed by Edgar et al. (Edgar et al., 2011), UCHIME is one of the most widely
256 used computational tools for detecting chimeric sequences in amplicon sequencing
257 data. The UCHIME algorithm detects chimeras by evaluating how well a query
258 sequence (Q) can be explained as a mosaic of two parent sequences (A and B)
259 from a reference database. The query sequence is first divided into four non-
260 overlapping segments or chunks. Each chunk is independently searched against a
261 reference database that is assumed to be free of chimeras. The best matches to
262 each segment are collected, and from these results, two candidate parent sequences
263 are identified, typically the two sequences that best explain all chunks of the query.
264 Then a three-way alignment among the query (Q) and the two parent candidates
265 (A and B) is done. From this alignment, UCHIME attempts to find a chimeric
266 model (M) which is a hypothetical recombinant sequence formed by concatenating
267 fragments from A and B that best match the observed Q

268 **Chimeric Alignment and Scoring**

269 To decide whether a query is chimeric, UCHIME computes several alignment-
270 based metrics between Q, its top hit (T, the most similar known sequence), and
271 the chimeric model (M). The key differences are measured as: dQT or the number
272 of mismatches between the query and the top hit as well as dQM or the number
273 of mismatches between the query and the chimeric model. From these, a chimera
274 score is calculated to quantify how much better the chimeric model fits the query
275 compared to a single parent. If the model's similarity to Q exceeds a defined
276 threshold (typically $\geq 0.8\%$ better identity), the sequence is reported as chimeric.
277 A higher score indicates stronger evidence of chimerism, while lower scores suggest
278 that the sequence is more likely to be authentic.

279 In de novo mode, UCHIME applies an abundance-driven strategy. Only se-
280 quences at least twice as abundant as the query are considered as potential parents.
281 Non-chimeric sequences identified at each step are added iteratively to a growing
282 internal database for subsequent queries.

283 **Limitations of UCHIME**

284 Although UCHIME was a significant advancement in chimera detection, it has
285 notable limitations. According to (Edgar, 2016) and the UCHIME practical notes
286 (Edgar, n.d), many of the accuracy results reported in the original 2011 paper
287 were overly optimistic due to unrealistic benchmark designs that assumed com-
288 plete reference coverage and perfect sequence quality. In practice, UCHIME's
289 accuracy can decline when (1) the reference database is incomplete or contains

290 erroneous entries; (2) low-divergence chimeras are present, as these closely resem-
291 ble genuine biological variants; (3) sequence datasets include residual sequencing
292 errors, leading to spurious alignments or misidentification; and (4) the abundance
293 ratio between parent and chimera is distorted by amplification bias. Additionally,
294 UCHIME tends to misclassify sequences as non-chimeric when parent sequences
295 are missing from the database. These limitations motivated the development of
296 UCHIME2.

297 **2.3.2 UCHIME2**

298 To overcome the limitations of its predecessor, UCHIME2 (Edgar, 2016) intro-
299 duced several methodological and algorithmic refinements that significantly en-
300 hanced the accuracy and reliability of chimera detection. One major improve-
301 ment lies in its approach to uncertainty handling. In earlier versions, sequences
302 with limited reference support were often incorrectly classified as non-chimeric,
303 increasing the likelihood of false negatives. UCHIME2 addresses this issue by
304 designating such ambiguous sequences as “unknown,” thereby providing a more
305 conservative and reliable classification framework.

306 Another notable advancement is the introduction of multiple application-
307 specific modes that allow users to tailor the algorithm’s performance to the
308 characteristics of their datasets. The following parameter presets: denoised,
309 balanced, sensitive, specific, and high-confidence, enable researchers to optimize
310 the balance between sensitivity and specificity according to the goals of their
311 analysis.

312 In comparative evaluations, UCHIME2 demonstrated superior detection per-
313 formance, achieving sensitivity levels between 93% and 99% and lower overall
314 error rates than earlier versions or other contemporary tools such as DECIPHER
315 and ChimeraSlayer. Despite these advances, the study also acknowledged a fun-
316 damental limitation in chimera detection: complete error-free identification is
317 theoretically unattainable. This is due to the presence of “perfect fake models,”
318 wherein genuine non-chimeric sequences can be perfectly reconstructed from other
319 reference fragments. This underscore the uncertainty in differentiating authentic
320 biological sequences from artificial recombinants based solely on sequence similar-
321 ity, emphasizing the need for continued methodological refinement and cautious
322 interpretation of results.

323 2.3.3 CATch

324 As previously mentioned, UCHIME (Edgar et al., 2011) relied on alignment-based
325 sequences in amplicon data. However, researchers soon observed that different al-
326 gorithms often produced inconsistent predictions. A sequence might be identified
327 as chimeric by one tool but classified as non-chimeric by another, resulting in
328 unreliable filtering outcomes across studies.

329 To address these inconsistencies, Mysara, Saeys, Leys, Raes, and Monsieurs
330 (2015) developed the Classifier for Amplicon Tool Chimeras (CATCh), which rep-
331 resents the first ensemble machine learning system designed for chimera detection
332 in 16S rRNA amplicon sequencing. Rather than depending on a single detec-
333 tion strategy, CATCh integrates the outputs of several established tools, includ-
334 ing UCHIME, ChimeraSlayer, DECIPHER, Pintail, and Perseus. The individual

335 scores and binary decisions generated by these tools are used as input features for
336 a supervised learning model. The algorithm employs a Support Vector Machine
337 (SVM) with a Pearson VII Universal Kernel (PUK) to determine optimal weight-
338 ings among the input features and to assign each sequence a probability of being
339 chimeric.

340 Benchmarking in both reference-based and de novo modes demonstrated signif-
341 icant performance improvements. CATCh achieved sensitivities of approximately
342 85 percent in reference-based mode and 92 percent in de novo mode, with corre-
343 sponding specificities of approximately 96 percent and 95 percent. These results
344 indicate that CATCh detected 7 to 12 percent more chimeras than any individual
345 algorithm while maintaining high precision.

346 2.3.4 ChimPipe

347 Among the available tools for chimera detection, ChimPipe is a pipeline developed
348 to identify chimeric sequences such as biological chimeras. It uses both discordant
349 paired-end reads and split-read alignments to improve the accuracy and sensitivity
350 of detecting biological chimeras (Rodriguez-Martin et al., 2017). By combining
351 these two sources of information, ChimPipe achieves better precision than meth-
352 ods that depend on a single type of indicator.

353 The pipeline works with many eukaryotic species that have available genome
354 and annotation data (Rodriguez-Martin et al., 2017). It can also predict multiple
355 isoforms for each gene pair and identify breakpoint coordinates that are useful
356 for reconstructing and verifying chimeric transcripts. Tests using both simulated

357 and real datasets have shown that ChimPipe maintains high accuracy and reliable
358 performance.

359 ChimPipe lets users adjust parameters to fit different sequencing protocols or
360 organism characteristics. Experimental results have confirmed that many chimeric
361 transcripts detected by the tool correspond to functional fusion proteins, demon-
362 strating its utility for understanding chimera biology and its potential applications
363 in disease research (Rodriguez-Martin et al., 2017).

364 **2.4 Machine Learning Approaches for Chimera 365 and Sequence Quality Detection**

366 Traditional chimera detection tools rely primarily on heuristic or alignment-based
367 rules. Recent advances in machine learning (ML) have demonstrated that models
368 trained on sequence-derived features can effectively capture compositional and
369 structural patterns in biological sequences. Although most existing ML systems
370 such as those used for antibiotic resistance prediction, taxonomic classification,
371 or viral identification are not specifically designed for chimera detection, they
372 highlight how data-driven models can outperform similarity-based heuristics by
373 learning intrinsic sequence signatures. In principle, ML frameworks can integrate
374 indicators such as k-mer frequencies, GC-content variation and split-alignment
375 metrics to identify subtle anomalies that may indicate a chimeric origin (Arango
376 et al., 2018; Liang, Bible, Liu, Zou, & Wei, 2020; Ren et al., 2020).

377 2.4.1 Feature-Based Representations of Genomic Se- 378 quences

In genomic analysis, feature extraction converts DNA sequences into numerical representations suitable for ML algorithms. A common approach is k-mer frequency analysis, where normalized k-mer counts form the feature vector (Vervier, Mahé, Tournoud, Veyrieras, & Vert, 2015). These features effectively capture local compositional patterns that often differ between authentic and chimeric reads.

In particular, deviations in k-mer profiles between adjacent read segments can serve as a compositional signature of template-switching events. Additional descriptors such as GC content and sequence entropy can further distinguish sequence types; in metagenomic classification and virus detection, k-mer-based features have shown strong performance and robustness to noise (Ren et al., 2020; Vervier et al., 2015). For chimera detection specifically, abrupt shifts in GC or k-mer composition along a read can indicate junctions between parental fragments. Windowed feature extraction enables models to capture these discontinuities that rule-based algorithms may overlook.

Machine learning models can also leverage alignment-derived features such as the frequency of split alignments, variation in mapping quality, and local coverage irregularities. Split reads and discordant read pairs are classical indicators of genomic junctions and have been formalized in probabilistic frameworks for structural-variant discovery that integrate multiple evidence types (Layer, Hall, & Quinlan, 2014). Similarly, long-read tools such as Sniffles employ split-alignment and coverage anomalies to accurately localize breakpoints (Sedlazeck et al., 2018). Modern aligners such as Minimap2 (Li, 2018) output supplementary (SA tags) and

401 secondary alignments as well as chaining and alignment-score statistics that can
402 be summarized into quantitative predictors for machine-learning models. These
403 alignment-signal features are particularly relevant to PCR-induced mitochondrial
404 chimeras, where template-switching events produce reads partially matching dis-
405 tinct regions of the same or related genomes. Integrating such cues within a
406 supervised-learning framework enables artifact detection even in datasets lacking
407 complete or perfectly assembled references.

408 A further biologically grounded descriptor is the length of microhomology at
409 putative junctions. Microhomology refers to short, shared sequences, often in the
410 range of a few to tens of base pairs that are near breakpoints where template-
411 switching events typically happen. Studies of double strand break repair and
412 structural variation have demonstrated that the length of microhomology corre-
413 lates with the likelihood of microhomology-mediated end joining (MMEJ) or fork-
414 stalled template-switching pathways (Sfeir & Symington, 2015). In the context of
415 PCR-induced chimeras, template switching during amplification often leaves short
416 identical sequences at the junction of two concatenated fragments. Quantifying
417 the longest exact suffix-prefix overlap at each candidate breakpoint thus provides
418 a mechanistic signature of chimerism and complements both compositional (k-
419 mer) and alignment (SA count) features.

420 2.5 Synthesis of Chimera Detection Approaches

421 To provide an integrated overview of the literature discussed in this chapter, Ta-
422 ble 2.1 summarizes the major chimera detection studies, their methodological

⁴²³ approaches, and their known limitations.

Table 2.1: Summary of Existing Methods and Research Gaps

Method/Study	Scope/Approach	Limitations
Reference-based Chimera Detection	Compares query sequences against curated, non-chimeric reference databases; identifies mosaic sequences by evaluating similarity to known templates.	Depends heavily on completeness and quality of reference databases; often fails when novel taxa or missing parent sequences are present; reduced accuracy for low-divergence chimeras.
De novo Chimera Detection	Identifies chimeras using only internal dataset relationships; relies on abundance patterns and compositional similarity; reconstructs sequences as mosaics of high-abundance parents.	Assumes true sequences are more abundant—fails when amplification bias distorts abundance; struggles with evenly abundant parental sequences; can misclassify highly similar true variants.
UCHIME	Alignment-based chimera detection; segments query sequence, identifies parent candidates, performs 3-way alignment, and computes chimera scores; supports both reference-based and de novo modes.	Accuracy inflated in original benchmarks; suffers under incomplete databases; poor performance on low-divergence chimeras; sensitive to sequencing errors; misclassifies when parents are missing.
UCHIME2	Improved uncertainty handling; classifies ambiguous sequences as unknown; offers multiple sensitivity/specificity modes; more robust with incomplete references; higher sensitivity (93–99%).	Cannot achieve perfect accuracy due to “perfect fake models”; genuine variants may be indistinguishable from artificial recombinants; theoretical detection limit remains.
CATCh	First ML ensemble tool for 16S chimera detection; integrates outputs of UCHIME, ChimeraSlayer, DECIPHER, Pintail, Perseus via SVM classifier; significantly improves sensitivity and specificity.	Depends on performance of underlying tools; ML model limited to features they output; ensemble can still misclassify in datasets with extreme novelty or low coverage.
ChimPipe	Pipeline for detecting fusion genes and transcript-derived chimeras in	Designed for RNA-seq, not amplicons; needs high-quality genome

424 Across existing studies, no single approach reliably detects all forms of chimeric
425 sequences, particularly those generated by PCR-induced template switching in
426 mitochondrial genomes. Reference-based tools perform poorly when parental se-
427 quences are absent; de novo methods rely strongly on abundance assumptions;
428 alignment-based systems show reduced sensitivity to low-divergence chimeras; and
429 ensemble methods inherit the limitations of their component algorithms. RNA-
430 seq-oriented pipelines likewise do not generalize well to organelle data. Although
431 machine learning approaches offer promising feature-based detection, they are
432 rarely applied to mitochondrial genomes and are not trained specifically on PCR-
433 induced organelle chimeras. These limitations indicate a clear research gap: the
434 need for a specialized, feature-driven classifier tailored to mitochondrial PCR-
435 induced chimeras that integrates k-mer composition, split-alignment signals, and
436 micro-homology features to achieve more accurate detection than current heuristic
437 or alignment-based tools.

⁴³⁸ **Chapter 3**

⁴³⁹ **Research Methodology**

⁴⁴⁰ This chapter outlines the steps involved in completing the study, including data
⁴⁴¹ gathering, generating simulated mitochondrial Illumina reads, preprocessing and
⁴⁴² indexing the data, developing a bioinformatics pipeline to extract key features,
⁴⁴³ applying machine learning algorithms for chimera detection, and validating and
⁴⁴⁴ comparing model performance.

⁴⁴⁵ **3.1 Research Activities**

⁴⁴⁶ As illustrated in Figure 3.1, this study carried out a sequence of procedures to
⁴⁴⁷ detect PCR-induced chimeric reads in mitochondrial genomes. The process began
⁴⁴⁸ with collecting a mitochondrial reference sequence of *Sardinella lemuru* from the
⁴⁴⁹ National Center for Biotechnology Information (NCBI) database, which was used
⁴⁵⁰ as a reference for generating simulated clean and chimeric reads. These reads
⁴⁵¹ were subsequently indexed and mapped. The resulting collections then passed

452 through a bioinformatics pipeline that extracted k-mer profiles, supplementary
453 alignment (SA) features, and microhomology information to prepare the data for
454 model construction. The machine learning model was trained using the processed
455 input, and its precision and accuracy were assessed. It underwent tuning until it
456 reached the desired performance threshold, after which it proceeded to validation
457 and will undergo testing.

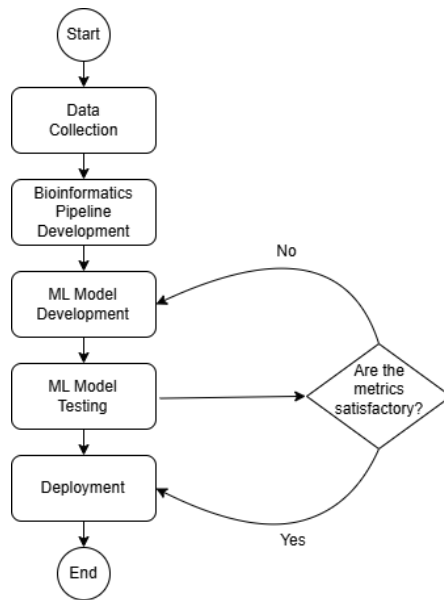


Figure 3.1: Process Diagram of Special Project

458 3.1.1 Data Collection

459 The mitochondrial genome reference sequence of *S. lemuru* was obtained from the
460 NCBI database (accession number NC_039553.1) in FASTA format. This sequence
461 served as the basis for generating simulated reads for model development.

462 This step was scheduled to begin in the first week of November 2025 and
463 expected to be completed by the end of that week, with a total duration of ap-

464 proximately one (1) week.

465 Data Preprocessing

466 To reduce manual repetition, all steps in the simulation and preprocessing pipeline
467 were executed using a custom script in Python (Version 3.11). The script runs
468 each stage, including read simulation, reference indexing, mapping, and alignment
469 processing, in a fixed sequence.

470 Sequencing data were simulated from the NCBI reference genome using `wgsim`
471 (Version 1.13). First, a total of 10,000 paired-end fragments were simulated,
472 producing 20,000 reads (10,000 forward and 10,000 reverse) from the the original
473 reference (`original_reference.fasta`) and and designated as clean reads using
474 the command:

```
475 wgsim -1 150 -2 150 -r 0 -R 0 -X 0 -e 0.001 -N 10000 \  
476           original_reference.fasta ref1.fastq ref2.fastq
```

477 The command parameters are as follows:

- 478 • `-1` and `-2`: read lengths of 150 base pairs for each paired-end read.
- 479 • `-r`, `-R`, `-X`: mutation rate, fraction of indels, and indel extension probability,
480 all set to a default value of 0.
- 481 • `-e`: base error rate, set to 0.001 to simulate realistic sequencing errors.
- 482 • `-N`: number of read pairs, set to 10,000.

483 Chimeric sequences were then generated from the same NCBI reference using a
484 separate Python script. Two non-adjacent segments were randomly selected such
485 that their midpoint distances fell within specified minimum and maximum thresh-
486 olds. The script attempts to retain microhomology, or short identical sequences
487 at segment junctions, to mimic PCR-induced template switching. The resulting
488 chimeras were written to `chimera_reference.fasta`, with headers recording seg-
489 ment positions and microhomology length. The `chimera_reference.fasta` was
490 processed with `wgsim` to simulate 10,000 paired-end fragments, generating 20,000
491 chimeric reads (10,000 forward reads in `chimeric1.fastq` and 10,000 reverse reads
492 in `chimeric2.fastq`) using the command format.

493 Next, a `minimap2` index of the reference genome was created using:

```
494 minimap2 -d ref.mmi original_reference.fasta
```

495 Minimap2 (Version 2.28) is a tool used to map reads to a reference genome.
496 The index `ref.mmi` of the original reference sequence is required by `minimap2` for
497 efficient read mapping. Mapping allows extraction of alignment features from each
498 read, which were used as input for the machine learning model. The simulated
499 clean and chimeric reads were then mapped to the reference index as follows:

```
500 minimap2 -ax sr -t 8 ref.mmi ref1.fastq ref2.fastq > clean.sam
```

```
501 minimap2 -ax sr -t 8 ref.mmi \  
502 chimeric1.fastq chimeric2.fastq > chimeric.sam
```

503 Here, `-ax sr` specifies short-read alignment mode, and `-t 8` uses 8 CPU

504 threads. The resulting clean and chimeric SAM files contain the alignment posi-
505 tions of each read relative to the original reference genome.

506 The SAM files were then converted to BAM format, sorted, and indexed using
507 `samtools` (Version 1.20):

```
508 samtools view -bS clean.sam -o clean.bam  
509 samtools view -bS chimeric.sam -o chimeric.bam  
510  
511 samtools sort clean.bam -o clean.sorted.bam  
512 samtools index clean.sorted.bam  
513  
514 samtools sort chimeric.bam -o chimeric.sorted.bam  
515 samtools index chimeric.sorted.bam
```

516 BAM files are the compressed binary version of SAM files, which enables faster
517 processing and reduced storage. Sorting arranges reads by genomic coordinates,
518 and indexing allows detection of SA as a feature for the machine learning model.

519 The total number of simulated reads was expected to be 40,000. The final col-
520 lection of reads contained 19,984 clean reads and 20,000 chimeric reads (39,984 en-
521 tries in total), providing a roughly balanced distribution between the two classes.
522 After alignment with `minimap2`, only 19,984 clean reads remained because un-
523 mapped reads were not included in the BAM file. Some sequences failed to align
524 due to the 5% error rate defined during `wgsim` simulation, which produced mis-
525 matches that caused certain reads to fall below the aligner's matching threshold.

526 This whole process is scheduled to start in the second week of November 2025

527 and is expected to be completed by the last week of November 2025, with a total
528 duration of approximately three (3) weeks.

529 **3.1.2 Bioinformatics Tools Pipeline**

530 A bioinformatics pipeline will be developed and implemented to extract the neces-
531 sary analytical features. This pipeline will function as a reproducible and modular
532 workflow that accepts FASTQ and BAM/SAM file inputs, processes them using
533 tools such as `samtools` and `jellyfish` (Version 2.3.1), and produces tabular fea-
534 ture matrices (TSV) for downstream machine learning. To ensure correctness
535 and adherence to best practices, bioinformatics experts at the PGC Visayas will
536 be consulted to validate the pipeline design, feature extraction logic, and overall
537 data integrity. This stage of the study is scheduled to begin in the first week of
538 January 2026 and conclude by the last week of February 2026, with an estimated
539 total duration of approximately two (2) months.

540 The bioinformatics pipeline focuses on three principal features from the simu-
541 lated and aligned sequencing data: (1) supplementary alignment flag (SA count),
542 (2) k-mer composition difference between read segments, and (3) microhomology
543 length at potential junctions. Each of these features captures a distinct biological
544 or computational signature associated with PCR-induced chimeras.

545 **Supplementary Alignment Flag**

546 Supplementary alignment information will be assessed using the mapped and
547 sorted BAM files (`clean.sorted.bam` and `chimeric.sorted.bam`) generated

548 from the data preprocessing stage. Alignment summaries will be checked using
549 `samtools flagstat` to obtain preliminary quality-control statistics, including
550 counts of primary, secondary, and supplementary (SA) alignments.

551 Both BAM files will be converted to SAM format for detailed inspection of
552 reads in each file:

```
553 samtools view -h clean.sorted.bam -o clean.sorted.sam  
554 samtools view -h chimeric.sorted.bam -o chimeric.sorted.sam
```

555 The SAM output will be checked for reads containing the SA:Z flag, as it
556 denotes supplementary alignments. Reads exhibiting these or substantial soft-
557 clipped regions will be considered strong candidates for chimeric artifacts. A
558 custom Python script would be created to extract the alignment-derived features
559 and relevant metadata including mapping quality, SAM flag information, CIGAR-
560 based clipping, and alignment coordinates. These extracted attributes would then
561 be organized and compiled into a TSV (.tsv) file.

562 K-mer Composition Difference

563 Chimeric reads often comprise fragments from distinct genomic regions, resulting
564 in a compositional discontinuity between segments. Comparing k-mer frequency
565 profiles between the left and right halves of a read allows detection of such abrupt
566 compositional shifts, independent of alignment information. This will be obtained
567 using Jellyfish, a fast k-mer counting software. For each read, the sequence will
568 be divided into two segments, either at the midpoint or at empirically determined
569 breakpoints inferred from supplementary alignment data, to generate left and right

570 sequence segments. Jellyfish will then compute k-mer frequency profiles (with $k =$
571 5 or 6) for each segment. The resulting k-mer frequency vectors will be normalized
572 and compared using distance metrics such as cosine similarity or Jensen–Shannon
573 divergence to quantify compositional disparity between the two halves of the same
574 read. The resulting difference scores will be stored in a structured TSV file.

575 Microhomology Length

576 The microhomology length was computed as part of the bioinformatics pipeline.
577 For each aligned read in the BAM files, the script first inferred a breakpoint
578 using the function `infer_breakpoint`, which represents a junction between two
579 segments. Breakpoints were determined primarily from soft-clipping patterns.
580 If no soft clips were present, SA tags were used to identify potential alignment
581 discontinuities.

582 Once a breakpoint was established, the script scanned a ± 40 base pair window
583 surrounding the breakpoint and used the function `longest_suffix_prefix_overlap`
584 to identify the longest exact suffix-prefix overlap between the left and right read
585 segments. This overlap, which represents consecutive bases shared at the junc-
586 tion, was recorded as the microhomology length. Additionally, the GC content
587 of the overlapping sequence was calculated using the function `gc_content`, which
588 counts guanine (G) and cytosine (C) bases within the detected microhomology
589 and divides by the total length, yielding a proportion between 0 and 1.

590 Short microhomologies, typically 3-20 base pairs in length, are recognized sig-
591 natures of PCR-induced template switching and can promote template recombi-
592 nation (Peccoud et al., 2018). Each read was annotated after capturing both the

593 length and GC content of microhomology.

594 3.1.3 Machine Learning Model Development

595 After feature extraction, the per-read feature matrices for clean and chimeric
596 reads were merged into a single dataset. Each row corresponded to one paired-
597 end read, and columns encoded alignment-structure features (e.g., supplementary
598 alignment count and spacing between segments), CIGAR-derived soft-clipping
599 statistics (e.g., left and right soft-clipped length, total clipped bases), k-mer com-
600 position discontinuity between read segments, and microhomology descriptors
601 near candidate junctions. The resulting feature set was restricted to quantities
602 that can be computed from standard BAM/FASTQ files in typical mitochondrial
603 sequencing workflows.

604 The labelled dataset was randomly partitioned into training (80%) and test
605 (20%) subsets using stratified sampling to preserve the 1:1 ratio of clean to
606 chimeric reads. Model development and evaluation were implemented in Python
607 (Version 3.11) using the `scikit-learn`, `xgboost`, `lightgbm`, and `catboost` li-
608 braries. A broad panel of classification algorithms was then benchmarked on the
609 training data to obtain a fair comparison of different model families under identical
610 feature conditions. The panel included: a trivial dummy classifier, L2-regularized
611 logistic regression, a calibrated linear support vector machine (SVM), k -nearest
612 neighbours, Gaussian Naïve Bayes, decision-tree ensembles (Random Forest, Ex-
613 tremely Randomized Trees, and Bagging with decision trees), gradient boosting
614 methods (Gradient Boosting, XGBoost, LightGBM, and CatBoost), and a shallow
615 multilayer perceptron (MLP).

616 For each model, five-fold stratified cross-validation was performed on the train-
617 ing set. In every fold, four-fifths of the data were used for fitting and the remaining
618 one-fifth for validation. Mean cross-validation accuracy, precision, recall, F1-score
619 for the chimeric class, and area under the receiver operating characteristic curve
620 (ROC–AUC) were computed to summarize performance and rank candidate meth-
621 ods. This baseline screen allowed comparison of linear, probabilistic, neural, and
622 ensemble-based approaches and identified tree-based ensemble and boosting mod-
623 els as consistently strong performers relative to simpler baselines.

624 **3.1.4 Model Benchmarking, Hyperparameter Optimiza-
625 tion, and Evaluation**

626 Model selection and refinement proceeded in two stages. First, the cross-validation
627 results from the broad panel were used to identify a subset of competitive mod-
628 els for more detailed optimization. Specifically, ten model families were carried
629 forward: L2-regularized logistic regression, calibrated linear SVM, Random For-
630 est, ExtraTrees, Gradient Boosting, XGBoost, LightGBM, CatBoost, Bagging
631 with decision trees, and a shallow MLP. This subset spans both linear and non-
632 linear decision boundaries, but emphasizes ensemble and boosting methods, which
633 showed superior F1 and ROC–AUC in the initial benchmark.

634 Second, hyperparameter optimization was conducted for each of the ten se-
635 lected models using randomized search with five-fold stratified cross-validation
636 (`RandomizedSearchCV`). For tree-based ensembles, the search space included the
637 number of trees, maximum depth, minimum samples per split and leaf, and the
638 fraction of features considered at each split. For boosting methods, key hyper-

639 parameters such as the number of boosting iterations, learning rate, tree depth,
640 subsampling rate, and column subsampling rate were tuned. For the MLP, the
641 number and size of hidden layers, learning rate, and L_2 regularization strength
642 were varied. In all cases, the primary optimisation criterion was the F1-score of
643 the chimeric class, averaged across folds.

644 For each model family, the hyperparameter configuration with the highest
645 mean cross-validation F1-score was selected as the best-tuned estimator. These
646 tuned models were then refitted on the full training set and evaluated once on the
647 held-out test set to obtain unbiased estimates of performance. Test-set metrics in-
648 cluded accuracy, precision, recall, F1-score for the chimeric class, and ROC–AUC.
649 Confusion matrices and ROC curves were generated for the top-performing mod-
650 els to characterise common error modes, such as false negatives (missed chimeric
651 reads) and false positives (clean reads incorrectly labelled as chimeric). The final
652 model or small set of models for downstream interpretation was chosen based on
653 a combination of test-set F1-score, ROC–AUC, and practical considerations such
654 as model complexity and ease of deployment within a bioinformatics pipeline.

655 3.1.5 Feature Importance and Interpretation

656 To relate model decisions to biologically meaningful signals, feature-importance
657 analyses were performed on the best-performing tree-based models. Two comple-
658 mentary approaches were used. First, built-in importance measures from ensemble
659 methods (e.g., split-based importances in Random Forest and Gradient Boosting)
660 were examined to obtain an initial ranking of features based on their contribution
661 to reducing impurity. Second, model-agnostic permutation importance was com-

662 puted on the test set by repeatedly permuting each feature column while keeping
663 all others fixed and measuring the resulting decrease in F1-score. Features whose
664 permutation led to a larger performance drop were interpreted as more influential
665 for chimera detection.

666 For interpretability, individual features were grouped into four conceptual
667 families: (i) supplementary alignment and alignment-structure features (e.g., SA
668 count, spacing between alignment segments, strand consistency), (ii) CIGAR-
669 derived soft-clipping features (e.g., left and right soft-clipped length, total clipped
670 bases), (iii) k-mer composition discontinuity features (e.g., cosine distance and
671 Jensen–Shannon divergence between k-mer profiles of read segments), and (iv) mi-
672 crohomology descriptors (e.g., microhomology length and local GC content around
673 putative breakpoints). Aggregating permutation importance scores within each
674 family allowed assessment of which biological signatures contributed most strongly
675 to the classifier’s performance. This analysis provided a basis for interpreting the
676 trained models in terms of known mechanisms of PCR-induced template switching
677 and for identifying which alignment- and sequence-derived cues are most informa-
678 tive for distinguishing chimeric from clean mitochondrial reads.

679 3.1.6 Validation and Testing

680 Validation will involve both internal and external evaluations. Internal valida-
681 tion was achieved through five-fold cross-validation on the training data to verify
682 model generalization and reduce variance due to random sampling. External vali-
683 dation will be achieved through testing on the 20% hold-out dataset derived from
684 the simulated reads, which will be an unbiased benchmark to evaluate how well

685 the trained models generalized to unseen data. All feature extraction and pre-
686 processing steps were performed using the same bioinformatics pipeline to ensure
687 consistency and comparability across validation stages.

688 Comparative evaluation was performed across all candidate algorithms, in-
689 cluding a trivial dummy classifier, L2-regularized logistic regression, a calibrated
690 linear SVM, k-nearest neighbours, Gaussian Naïve Bayes, decision-tree ensembles,
691 gradient boosting methods, and a shallow MLP. This evaluation determined which
692 models demonstrated the highest predictive performance and computational effi-
693 ciency under identical data conditions. Their metrics were compared to identify
694 which algorithms were most suitable for further refinement.

695 3.1.7 Documentation

696 Comprehensive documentation was maintained throughout the study to ensure
697 transparency and reproducibility. All stages of the research, including data gath-
698 ering, preprocessing, feature extraction, model training, and validation, were sys-
699 tematically recorded in a `.README` file in the GitHub repository. For each ana-
700 lytical step, the corresponding parameters, software versions, and command line
701 scripts were documented to enable exact replication of results.

702 The repository structure followed standard research data management prac-
703 tices, with clear directories for datasets and scripts. Computational environments
704 were standardized using Conda, with an environment file (`environment.arm.yml`)
705 specifying dependencies and package versions to maintain consistency across sys-
706 tems.

707 For manuscript preparation and supplementary materials, Overleaf (L^AT_EX)
708 was used to produce publication-quality formatting and consistent referencing. f

709 3.2 Calendar of Activities

710 Table 3.1 presents the project timeline in the form of a Gantt chart, where each
711 bullet point corresponds to approximately one week of planned activity.

Table 3.1: Timetable of Activities

Activities (2025)	Nov	Dec	Jan	Feb	Mar	Apr	May
Data Collection and Simulation	• • •						
Bioinformatics Tools Pipeline			• • •	• • •			
Machine Learning Development			• •	• • •	• • •	• •	
Testing and Validation						• •	• • •
Documentation	• • •	• • •	• • •	• • •	• • •	• • •	• • •

⁷¹² References

- ⁷¹³ Anderson, S., Bankier, A., Barrell, B., Bruijn, M., Coulson, A., Drouin, J., ...
⁷¹⁴ Young, I. (1981, 04). Sequence and organization of the human mitochondrial
⁷¹⁵ genome. *Nature*, *290*, 457-465. doi: 10.1038/290457a0
- ⁷¹⁶ Arango, G., Garner, E., Pruden, A., Heath, L., Vikesland, P., & Zhang, L. (2018,
⁷¹⁷ 02). Deeparg: A deep learning approach for predicting antibiotic resistance
⁷¹⁸ genes from metagenomic data. *Microbiome*, *6*. doi: 10.1186/s40168-018
⁷¹⁹ -0401-z
- ⁷²⁰ Bentley, D. R., Balasubramanian, S., Swerdlow, H. P., Smith, G. P., Milton, J.,
⁷²¹ Brown, C. G., ... Smith, A. J. (2008). Accurate whole human genome
⁷²² sequencing using reversible terminator chemistry. *Nature*, *456*(7218), 53–
⁷²³ 59. doi: 10.1038/nature07517
- ⁷²⁴ Boore, J. L. (1999). Animal mitochondrial genomes. *Nucleic Acids Research*,
⁷²⁵ *27*(8), 1767–1780. doi: 10.1093/nar/27.8.1767
- ⁷²⁶ Cameron, S. L. (2014). Insect mitochondrial genomics: Implications for evolution
⁷²⁷ and phylogeny. *Annual Review of Entomology*, *59*, 95–117. doi: 10.1146/
⁷²⁸ annurev-ento-011613-162007
- ⁷²⁹ Dierckxsens, N., Mardulyn, P., & Smits, G. (2017). Novoplasty: de novo assembly
⁷³⁰ of organelle genomes from whole genome data. *Nucleic Acids Research*,

- 731 45(4), e18. doi: 10.1093/nar/gkw955
- 732 Edgar, R. C. (2016). Uchime2: improved chimera prediction for amplicon se-
733 quencing. *bioRxiv*. Retrieved from <https://api.semanticscholar.org/>
734 CorpusID:88955007
- 735 Edgar, R. C. (n.d.). Uchime in practice. Retrieved from https://www.drive5.com/usearch/manual7/uchime_practical.html
- 736 Edgar, R. C., Haas, B. J., Clemente, J. C., Quince, C., & Knight, R. (2011).
737 Uchime improves sensitivity and speed of chimera detection. *Bioinformatics*,
738 27(16), 2194–2200. doi: 10.1093/bioinformatics/btr381
- 740 Glenn, T. C. (2011). Field guide to next-generation dna sequencers. *Molecular
741 Ecology Resources*, 11(5), 759–769. doi: 10.1111/j.1755-0998.2011.03024.x
- 742 Gonzalez, J. M., Zimmermann, J., & Saiz-Jimenez, C. (2004, 09). Evalu-
743 ating putative chimeric sequences from pcr-amplified products. *Bioin-
744 formatics*, 21(3), 333-337. Retrieved from <https://doi.org/10.1093/bioinformatics/bti008>
745 doi: 10.1093/bioinformatics/bti008
- 746 Gray, M. W. (2012). Mitochondrial evolution. *Cold Spring Harbor perspectives
747 in biology*, 4. Retrieved from <https://doi.org/10.1101/cshperspect.a011403>
748 doi: 10.1101/cshperspect.a011403
- 749 Hahn, C., Bachmann, L., & Chevreux, B. (2013). Reconstructing mitochondrial
750 genomes directly from genomic next-generation sequencing reads—a baiting
751 and iterative mapping approach. *Nucleic Acids Research*, 41(13), e129. doi:
752 10.1093/nar/gkt371
- 753 Jin, J.-J., Yu, W.-B., Yang, J., Song, Y., dePamphilis, C. W., Yi, T.-S., & Li,
754 D.-Z. (2020). Getorganelle: a fast and versatile toolkit for accurate de
755 novo assembly of organelle genomes. *Genome Biology*, 21(1), 241. doi:
756 10.1186/s13059-020-02154-5

- 757 Judo, M. S. B., Wedel, W. R., & Wilson, B. H. (1998). Stimulation and sup-
758 pression of pcr-mediated recombination. *Nucleic Acids Research*, *26*(7),
759 1819–1825. doi: 10.1093/nar/26.7.1819
- 760 Labrador, K., Agmata, A., Palermo, J. D., Ravago-Gotanco, R., & Pante, M. J.
761 (2021). Mitochondrial dna reveals genetically structured haplogroups of
762 bali sardinella (sardinella lemuru) in philippine waters. *Regional Studies in*
763 *Marine Science*, *41*, 101588. doi: 10.1016/j.rsma.2020.101588
- 764 Layer, R., Hall, I., & Quinlan, A. (2014, 10). Lumpy: A probabilistic framework
765 for structural variant discovery. *Genome Biology*, *15*. doi: 10.1186/gb-2014
766 -15-6-r84
- 767 Li, H. (2018, 05). Minimap2: pairwise alignment for nucleotide sequences. *Bioin-*
768 *formatics*, *34*(18), 3094-3100. Retrieved from <https://doi.org/10.1093/bioinformatics/bty191> doi: 10.1093/bioinformatics/bty191
- 770 Liang, Q., Bible, P. W., Liu, Y., Zou, B., & Wei, L. (2020, 02). Deepmi-
771 crobes: taxonomic classification for metagenomics with deep learning. *NAR*
772 *Genomics and Bioinformatics*, *2*(1), lqaa009. Retrieved from <https://doi.org/10.1093/nargab/lqaa009> doi: 10.1093/nargab/lqaa009
- 774 Metzker, M. L. (2010). Sequencing technologies — the next generation. *Nature*
775 *Reviews Genetics*, *11*(1), 31–46. doi: 10.1038/nrg2626
- 776 Mysara, M., Saeys, Y., Leys, N., Raes, J., & Monsieurs, P. (2015). Catch,
777 an ensemble classifier for chimera detection in 16s rrna sequencing stud-
778 ies. *Applied and Environmental Microbiology*, *81*(5), 1573-1584. Retrieved
779 from <https://journals.asm.org/doi/abs/10.1128/aem.02896-14> doi:
780 10.1128/AEM.02896-14
- 781 Peccoud, J., Lequime, S., Moltini-Conclois, I., Giraud, I., Lambrechts, L., &
782 Gilbert, C. (2018, 04). A survey of virus recombination uncovers canon-

- 783 ical features of artificial chimeras generated during deep sequencing li-
784 brary preparation. *G3 Genes—Genomes—Genetics*, 8(4), 1129-1138. Re-
785 trieved from <https://doi.org/10.1534/g3.117.300468> doi: 10.1534/
786 g3.117.300468
- 787 Qin, Y., Wu, L., Zhang, Q., Wen, C., Nostrand, J. D. V., Ning, D., ... Zhou, J.
788 (2023). Effects of error, chimera, bias, and gc content on the accuracy of
789 amplicon sequencing. *mSystems*, 8(6), e01025-23. Retrieved from <https://journals.asm.org/doi/abs/10.1128/msystems.01025-23> doi: 10.1128/
790 msystems.01025-23
- 791 Qiu, X., Wu, L., Huang, H., McDonel, P. E., Palumbo, A. V., Tiedje, J. M., &
792 Zhou, J. (2001). Evaluation of pcr-generated chimeras, mutations, and het-
793 eroduplexes with 16s rrna gene-based cloning. *Applied and Environmental
794 Microbiology*, 67(2), 880–887. doi: 10.1128/AEM.67.2.880-887.2001
- 795 Ren, J., Song, K., Deng, C., Ahlgren, N., Fuhrman, J., Li, Y., ... Sun, F. (2020,
796 01). Identifying viruses from metagenomic data using deep learning. *Quan-
797 titative Biology*, 8. doi: 10.1007/s40484-019-0187-4
- 798 Rodriguez-Martin, B., Palumbo, E., Marco-Sola, S., Griebel, T., Ribeca, P.,
799 Alonso, G., ... Djebali, S. (2017, 01). Chimpipe: Accurate detection of
800 fusion genes and transcription-induced chimeras from rna-seq data. *BMC
801 Genomics*, 18. doi: 10.1186/s12864-016-3404-9
- 802 Rognes, T., Flouri, T., Nichols, B., Quince, C., & Mahé, F. (2016). Vsearch: a
803 versatile open source tool for metagenomics. *PeerJ*, 4, e2584. doi: 10.7717/
804 peerj.2584
- 805 Sedlazeck, F., Rescheneder, P., Smolka, M., Fang, H., Nattestad, M., von Haeseler,
806 A., & Schatz, M. (2018, 06). Accurate detection of complex structural
807 variations using single-molecule sequencing. *Nature Methods*, 15. doi: 10
808

- 809 .1038/s41592-018-0001-7
- 810 Sfeir, A., & Symington, L. S. (2015). Microhomology-mediated end joining: A
811 back-up survival mechanism or dedicated pathway? *Trends in Biochemical
812 Sciences*, 40(11), 701-714. Retrieved from <https://www.sciencedirect.com/science/article/pii/S0968000415001589> doi: <https://doi.org/10.1016/j.tibs.2015.08.006>
- 813
- 814
- 815 Vervier, K., Mahé, P., Tournoud, M., Veyrieras, J.-B., & Vert, J.-P. (2015,
816 11). Large-scale machine learning for metagenomics sequence classifica-
817 tion. *Bioinformatics*, 32(7), 1023-1032. Retrieved from <https://doi.org/10.1093/bioinformatics/btv683> doi: 10.1093/bioinformatics/btv683
- 818
- 819 Willette, D., Bognot, E., Mutia, M. T., & Santos, M. (2011). *Biology and ecology
820 of sardines in the philippines: A review* (Vol. 13; Tech. Rep. No. 1). NFRDI
821 Technical Paper Series. Retrieved from <https://nfrdi.da.gov.ph/tpjf/etc/Willette%20et%20al.%20Sardines%20Review.pdf>
- 822